A High Step-Up Resonant Converter For Low and High Input Voltage Applications

Preetha[1],Z.Shiqnaas Gaanam[2],M.Annapoorani[3],K.Veeralakshmi[4]

UG students,Department of EEE,VCET,Madurai,Tamil Nadu[1][2][3]

Assistant Professor,Department of EEE,VCET,Madurai,Tamil Nadu[4]

Abstract – A high voltage gain dc-dc converter is introduced in this paper. The proposed topology resembles full bridge inverter on input side while having isolated resonant converter based voltage multiplier rectifier on its output side, which can operate either in buck mode or boost mode could be more flexible. This converter offers continuous input current makes it more appealing for the integeration of renewable sources like solar panels to a 400-V dc bus. Also, the proposed converter is capable of drawing power from either a single source or two independent sources. Furthermore, the voltage multiplier used offers low voltage rating of capacitors which potentially leads to size reduction .The converter design and component selection has been discussed in detail with supporting simulation results. A hardware prototype of proposed converter with Vin =20V and Vout =400V has been developed to validate the analytical results.

Index terms **– Full bridge inverter, Isolated Resonant Converter, Voltage Multiplier rectifier, high-voltage-gain dc-dc power electronics converter.**

I.INTRODUCTION

Distribution systems at 400-V dc have been gaining popularity as they offer better efficiency, higher reliability at an improved power quality, and low cost compared to ac distribution systems[1-4]. They offer a simpler integration of renewable energy and energy storage systems. Currently, telecom centers, data centers, commercial buildings, residential buildings, and microgrids are among the emerging examples of dc distribution systems[5-7]. One of the challenges facing such systems is the power electronic converters for integrating renewable

sources into the 400-V dc bus. A typical voltage range for solar panels is between 20V dc to 40V dc.

Stepping up these voltages to 400-V dc using classic boost and buck-boost converters requires high duty ratios which results in high component stress and

lower efficiency.Therefore, a typical choice would be using two cascaded converters; which results in inefficientoperation, reduced reliability, increased size, and stability issues.Isolated topologies like

flyback, forward, half-bridge, full- bridge, and push-

pull converters have discontinuous input currents a hence would require large inputcapacitors.

High-voltage-gain dc-dc converters using a boost

stagefollowed by voltage multiplier (VM) cells have been proposed in [8-11]. The second order hybrid boosting converter proposed in [8] offers relatively low voltage gain in comparison to its voltage multiplier component count. It also has a very large input current ripple in proportion to its average. High step-up converters using single-inductor-energy-storage-cell-based switched capacitors proposed in [9] do not offer voltage gains high enough to boost a 20V input to 400V at an reasonable switching duty cycle. The multiple-inductor-energy-storage-cell-based switched capacitor based high voltage converters [9]offer a relatively low voltage gain in proportion to its component count. The switched-capacitor-based active-network converter proposed in [10] has a discontinuous input current ripple due to the series and parallel connection of the inductors in its two modes of operation. The transformer-less high-gain boost converter proposed in [11] offers continuous input current but the switches experience a high voltagestress.

High-voltage-gain dc-dc converters using coupled inductors and high frequency transformers have been proposed for the integration of solar panels to 400V dc bus [12-18]. In such converters, the design of high frequency transformers and coupled inductors is complicated as the leakage inductance increases when higher voltage

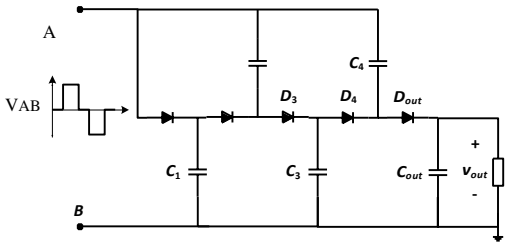

(a) Dickson charge pump[19]

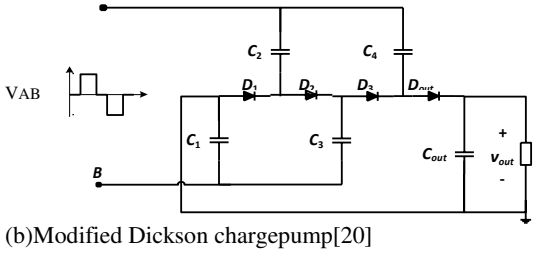

(b)Modified Dickson chargepump[20]

Fig 1.Conventional and modified Dickson charge pump voltage multiplier circuits

gains are intended. As a result, the converter switches experience large voltage spikes and therefore would require clamping circuitry to reduce the voltage stress on the switches. These clamping circuits have a negative effect on the converter voltage gains. A family of non-isolated high-voltage-gain dc-dc converters that makes use of VM cells derived from the Dickson charge pump (a) has been proposed in [19]. The voltage rating of each VM cell capacitor is twice that of its previous VM cell. Also, the inductors (L1, L2) and switches (S1, S2) experience different current stresses whenever even number of VM cells is used.

The converter offers continuous input current and low voltage stress (1/4th of its output voltage) on its switches. This converter can draw power from a single source or two independent sources while having continuous input currents, which makes it suitable for applications like solar panels. The converter requires lower voltage rating capacitors for its VM circuit and also one less diode. The inductors and switches experience identical current stresses making the component selection process for the converter simpler has been proposed in [20].

Isolated high step up converters are being preferred due to their galvanic isolation capabilities between the source and the load sides , since the isolated converts prefer the transformer based isolation , the efficiency is greatly depend up on it, without transformers the isolation part is cannot be determined. But in occasions that if the transformer can be operated at its maximum resonated condition the maximum , hence a resonant converter would be an preferred choice , in this project a resonant converter based step up and step down converter with a high gain and efficiency is being proposed.

In section II, Resonant Voltage-Multiplier Rectifier is been proposed. Section III introduces modes of operations. The voltage gain of proposed conveter has been derived in section IV. Section V concludes the paper. A comparative analysis of the proposed converter and the high-voltage-gain converter shown.

II.RESONANT VOLTAGE-MULTIPLIER RECTIFIER

The topologies of the conventional RVMR are shown in Fig. 4.1, where $C_{r1}$and C_{r2} are resonant capacitors, $L_r$is a resonant inductor, $D_1$and $D_4$are output diodes, D_2 and $D_4$are regenerative diodes, T is a high frequency transformer (only the secondary-winding is shown), and $S_1$and $S_2$are the active switches through which the output power can be regulated. The resonant tank is composed of three elements,C_{r1},$C_{r2}$and L_r. In the N-Type RVMR, the two switches $S_1$and $S_2$are placed on the underside of the rectifier and connected to the negative potential of the output voltage V_0, as shown in Fig. 2(a), while in the P-Type RVMR, the two switches are connected to the positive potential of theV_0, as illustrated in Fig. 2(b). The operation principles of the two RVMRs are the same, but an easier gate drive can be achieved with the N-Type RVMR because the two switches are referenced to the

output ground

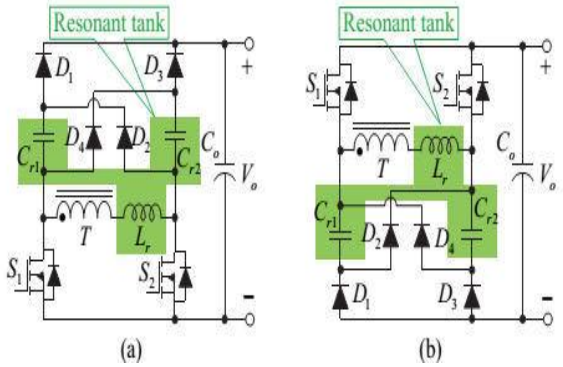

Fig 2: Conventional resonant voltage multiplier rectifiers, (a) N-Type, (b) P-Type

Different from traditional RC topologies that using variable frequency control to regulate output power, the resonant tank in the RVMR always operates at the resonant frequency determined by the following equation.

$$f_r = \frac{\omega_r}{2\pi} = \frac{1}{2\pi\sqrt{L_r(C_{r1}+C_{r2})}} \quad (1)$$

When the switches in the RVMR are ON, the voltage on the secondary-winding of the transformer is directly applied on the resonant inductor, in which case, the resonant inductor acts as a boost inductor. When the switches turn off, the inductor resonates with the capacitors. The operation makes the initial conditions of the resonant process to be set, allowing the output power to be regulated. Therefore, for good operation of the RVMR, the transformer Should be able to generate high frequency voltage, which is a basic requirement of the RVMR. This can be realized by introducing a primary-side circuit properly, i.e. the voltage fed full-bridge circuit or three-level circuit shown in Fig.2(a)and2(b) The choice of the primary-side circuit is dependent on the requirement of practical applications and not limited to those shown in Fig. 3. RCs can be derived by combining a proper primary-side circuit and the proposed RVMR. An example topology with full-bridge input stage and N-type RVMR is shown in Fig.4

The main focus of existing approach is the RVMR. Thefull-bridge RC shown in Fig. 5 is taken as an example and to be analyzed to explain the control and operation principles. In Fig. 4.4, the inductor Lmis the magnetizing inductance of the transformer, and n is the secondary to primary turns ratio of the transformer T. Lmdoesn't participate in the resonant or the power transferring of the converter, but it can help to realize soft-switching of the primary side switches.

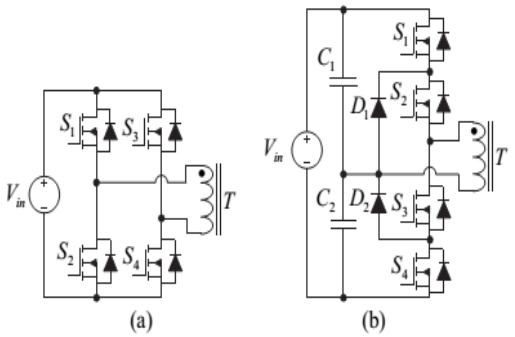

Fig.3. Primary-side circuit candidates, (a) Full-bridge, (b) three-level.

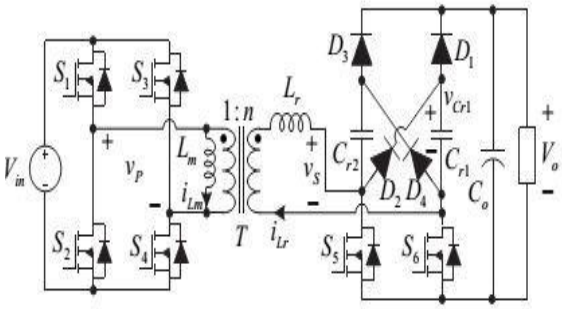

Fig 4: A full-bridge resonant converter based on the N-type RVMR

III.TOPOLOGY AND MODES OF OPERATION

The main focus of existing approach is the RVMR. In practice, the leakage inductance of the transformer Tis used as a part of the resonant inductanceL_r. The resonant capacitors $C_{r1}$and $C_{r2}$are not only used as a part of the resonant tank, but also used to double the output voltage, which is similar to the voltage multiplier in the interleaved Boost converter. The average voltage across $C_{r1}$and $C_{r2}$is only half of the output voltage. For simplicity, normalized voltage gain Gis defined as

$$G = \frac{V_o}{2nV_{in}} \quad (2)$$

and operation modes of the converter are defined to be buck mode (G<1) and boost mode (G≥1) according to the range of G. All switches operate at the resonant frequency determined by (1). Phase-shift control strategy is employed to regulate the output voltage and power. The primary-side phase-shift angle,φ_P, is defined to be the phase difference between the gate signals of$S_1$and S_4, while the secondary-side phase-shift angle, φ_S, is defined to be the phase difference between the gate signals of$S_4$and S_6. For simplicity,

equivalent primary-side andsecondary-side phase-shift duty cycles $d_{\varphi P}$and $d_{\varphi S}$are defined: $d_{\varphi P}=\frac{\varphi_P}{\pi}$, $d_{\varphi S}=\frac{\varphi_S}{\pi}$.

A. Boost Mode with Secondary-Side Phase-Shift Control:

When the voltage conversion ratio G≥1, the converter operates in the boost mode, in which, the primary-side duty cycle$d_{\varphi P}$is constant $d_{\varphi P}$=1, and the secondary-side duty cycle $d_{\varphi S}$is used to regulate the output voltage and power.The operation waveforms of the proposed converter with secondary-side phase-shift control are shown in Fig. 5. The steady state trajectory curve of the resonant inductor current i_{Lr}, and resonant capacitor voltage,v_{Cr1}, is shown in Fig. 6 for easily understanding the operation of the converter. To simplify the analysis, the inductor current is multiplied by the impedance of the resonant tank,Z_r, which is defined as follows

$$Z_r = \sqrt{\frac{L_r}{C_{r1}+C_{r2}}} = \sqrt{\frac{L_r}{2C_r}} \quad (3)$$

There are totally ten switching stages in one switching cycle. Due to the symmetry of the operation, only half of the switching cycle, Stage1~Stage5, are analyzed here. The equivalent circuit of each switching stage is shown in Fig. 7.

Stage 1 [t0,t1] [Fig. 8(a)]: Before t0, the switches S2, S4 and S5 are ON, iLr has been reset to zero. At t0, S2 and S4 turn OFF, entering a period of dead time. The magnetizing inductor Lm acts as a current source during this short time period to discharge the drain-source voltages of the switches S1 and S4, resulting in ZVS of S2 and S4. Meanwhile, the input voltage is directly applied on the resonant inductor Lr. So the inductor current increases linearly and expressed as follows.(4.3)

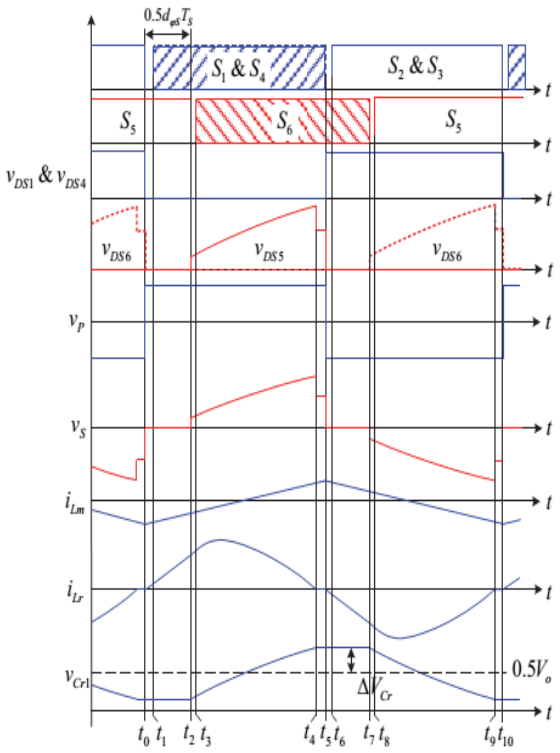

Fig 5. Key waveforms of the RC in the boost mode

$$i_{Lr}(t) = \frac{nV_{in}}{L_r}(t-t_0) \quad (4)$$

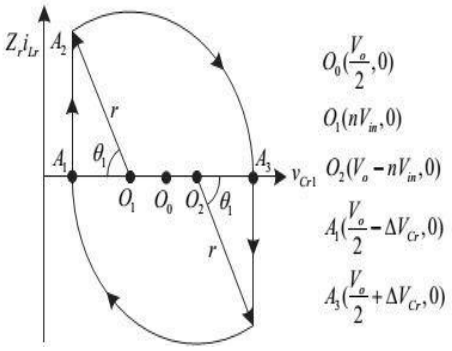

Fig 6: Trajectory curve of state variables of the resonant tank in boost mode

Stage 2 [t1, t2] [Fig. 8(b)]: At t1, S1and S4turns ON with ZVS.The equivalent circuit of the resonant inductor in the Stage 1 and Stage 2 is illustrated in Fig. 7(a), where the operation of the proposed RC is similar to a conventional PWM boost converter. From the view of the trajectory curve, the operating point moves along the trajectory curve from point A1to point A2, as shown in Fig. 6.

Stage 4 [t2, t4] [Fig. 8(c)]: At t2, S5turns OFF. The current of Lrhas been charged to an initial condition and now the converter operates similar to a series-resonant

converter. $L_r$and the parallel combination of $C_{r1}$and C_{r2}begin to resonate. In this stage, the diodes D_2, D_4 and the body diode of $S_6$are ON.

Stage 4 [t_4, t_4] [Fig. 8(d)]: At t_4, $S_6$is turned on with ZVS. During State 4 and Stage 4, the capacitor $C_{r1}$is charged while $C_{r2}$is discharged. The equivalent circuit of the resonant tank of these two stages is illustrated in Fig. 7(b). The capacitor voltage always satisfies $v_{Cr1}=V_o-v_{Cr2}$, so the average voltage of the two capacitors are the same and satisfy $V_{Cr1}=V_{Cr2}=0.5V_o$. The resonant stage ends when the current i_{Lr}reaches zero and the diodes $D_2$and D_4turn OFF with zero-current and without reverse-recovery losses. In the resonant stage, the converter moves along the trajectory curve from point $A_2$to A_4in Fig. 6, and finally reaches A4at the end of Stage 4.

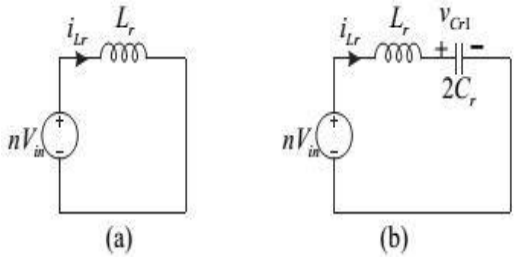

Fig 7: Equivalent circuits of (a) Stage 1 & Stage 2, (b) Stage 3 & Stage 4

The center pointaround which these states resonate, O_1, is located at (nV_{in},0). The current of $i_{Lr}$and voltage of $v_{Cr1}$are expressed as follows.

$$i_{Lr}(t_1)=\frac{nV_{in}d_{\varphi S}T_S}{L_r} \quad (5)$$

$$i_{Lr}(t)=\frac{r}{Z_r}\sin(\theta_1+\omega_r(t-t_1)) \quad (6)$$

$$v_{Cr1}(t)=nV_{in}-r\cos(\theta_1+\omega_r(t-t_1)) \quad (7)$$

Where,

$$r=\left|\frac{V_o}{2}-nV_{in}\right|+\Delta V_{Cr1} \quad (8)$$

$$\Delta V_{Cr1}=\frac{P_oT_S}{4V_oC_r} \quad (9)$$

$P_o$is the output power and $T_S$is the switching period.

Stage 5 [t_4, t_5] [Fig. 8(e)]: At t_4, i_{Lr}reaches zero, the converter enters an idle stage in which no power is being transferred to the load. From t_5, the other half switching cycle begins.

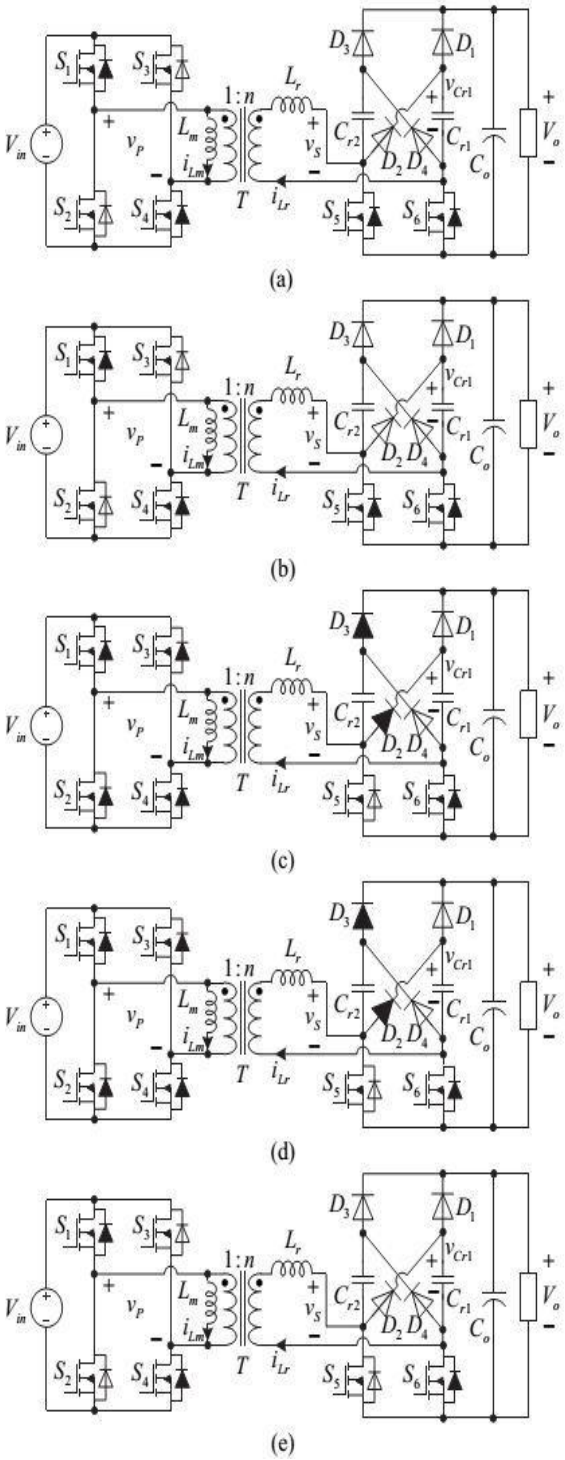

Fig 8: Equivalent circuits in different stages, (a) $[t_0, t_1]$, (b) $[t_1, t_2]$,(c) $[t_2, t_4]$, (d) $[t_4, t_4]$ and (e) $[t_4, t_5]$ (4.9)

B. Buck Mode with Primary-Side Phase-Shift Control

When the normalized voltage gain G≤1, the converter operates in the buck mode, in which, the secondary side phase-shift duty cycle $d_{\varphi S}$is zero, and the primary-side phase-shift duty cycle $d_{\varphi P}$is used to regulate the power flow.

The operation waveforms with primary-side phase-shift control are shown in Fig. 9, the steady state trajectory curve is shown in Fig. 10. There are totally five switching stages in half of the switching cycle. The equivalent circuit of each switching stage is shown in Fig.11.

Stage 1 [t_0, t_1] [Fig. 11(a)]: Before t_0, S_1, $S_4$and $S_5$are ON, i_{Lr}has resonated to zero. At t_0, S_4 and S_5turn OFF. $L_m$acts as a current source to discharge the drain-source voltage of S_4. So S_4can be turned ON under ZVS condition. Meanwhile, $L_r$and the parallel combination of $C_{r1}$and C_{r2}begin to resonate. The diodes D_2, D_4 and the body diode of $S_6$are ON.

Stage 2 [t1, t2] [Fig. 11(b)]: At t1, switches S4and S6turn ON with ZVS.

During Stage 1 and Stage 2, the converter operates similar to a conventional series resonant converter. The equivalent circuit of the resonant tank is shown in Fig. 12(a). $L_r$and the parallel combination of $C_{r1}$and C_{r2}resonate as the converter moves along the trajectory curve from point $A_1$to A_2in Fig. 10. $C_{r1}$is charged by $L_r$while $C_{r2}$is discharged.

The center point, around which these states resonate, O_1, is located at (nV_{in}, 0). The current of $i_{Lr}$and voltage of $v_{Cr1}$are expressed as

$$i_{Lr}(t) = \frac{r}{Z_r}\sin[\omega_r(t-t_0)] \quad (10)$$

$$v_{Cr1}(t) = nV_{in} - r\cos[\omega_r(t-t_0)] \quad (11)$$

Stage 4 [t_2, t_4] [Fig. 11(c)]: At t_2, $S_1$is OFF. The drain-source voltage of $S_2$is discharged by the magnetizing and resonantcurrents. So S2can be turned ON with ZVS.

Stage 4 [t_4, t_4] [Fig. 11(d)]: At t_4, S_2turns ON with ZVS. During Stage 4 and Stage 4, C_{r1}, $C_{r2}$and $L_r$resonate as the converter moves along the trajectory curve from point $A_2$to A_4in Fig. 4.9. The equivalent circuit of the resonant tank is shown in Fig. 4.11(b). The center point around which the variable states resonate is located at (0, 0). This stage ends when the current of $L_r$reaches zero and the rectifier diodes turn OFF with zero-current and without reverse-recovery losses.

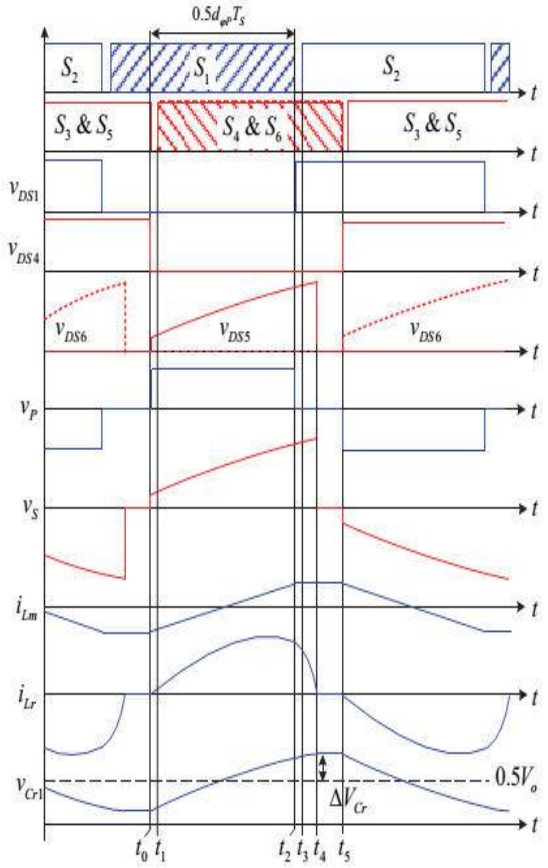

Fig 9: Key waveforms of the RC in the buck mode

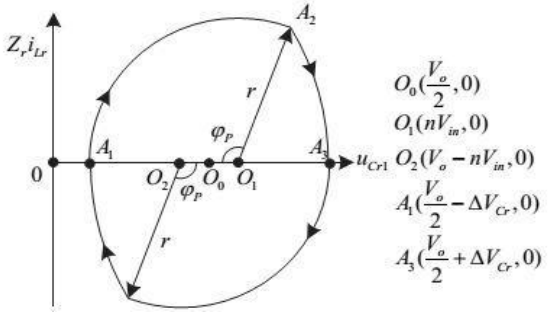

Fig 10. Trajectory curve of state variables of the resonant tank in buck mode

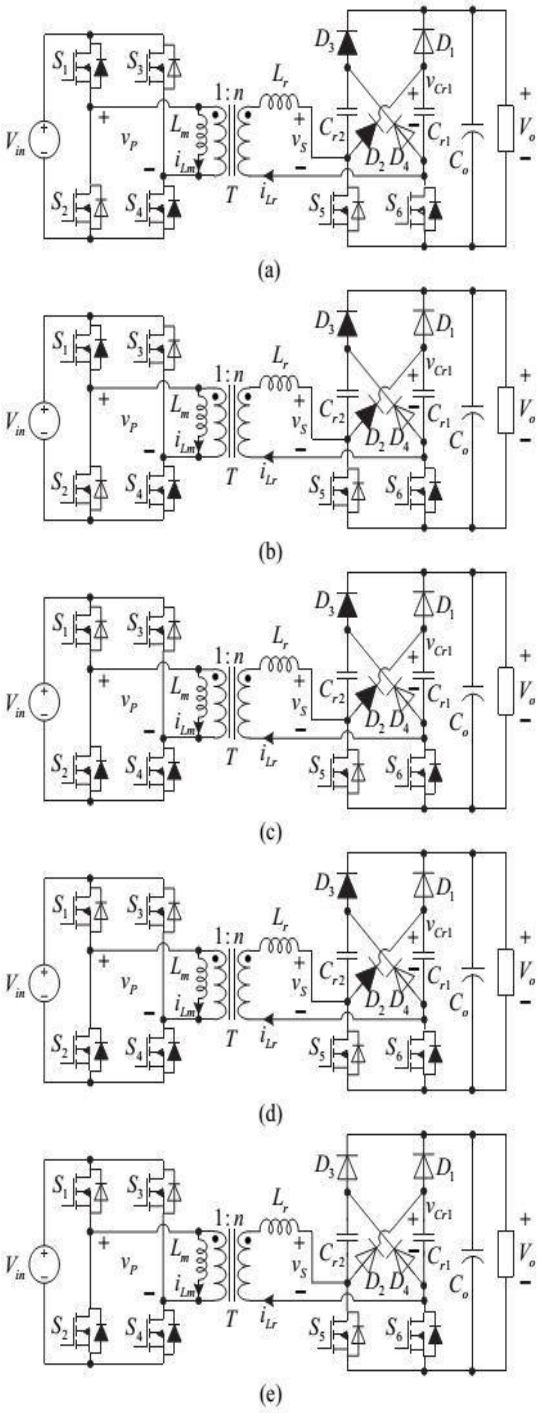

Fig 11: Equivalent circuits in different stages, (a) $[t_0, t_1]$, (b) $[t_1, t_2]$, (c) $[t_2, t_4]$, (d) $[t_4, t_4]$ and
(e) $[t_4, t_5]$

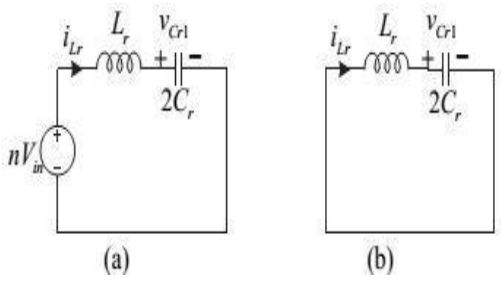

Fig 12: Equivalent circuits of (a) Stage 1 & Stage 2, (b) Stage 4 & Stage 4

Stage 5 [t_4, t_5] [Fig. 11(e)]: At t4, i_{Lr}reaches zero, the converter enters an idle stage. No power is being transferred to the load. From t_5, the other half switching cycle begins.

IV.CHARACTERISTICS AND DESIGNGUIDELINES

When the converter works in the boost mode with G≥1 and secondary-side phase-shift control, according to the operation principles and waveforms shown in Fig. 5 and Fig. 6, and ignoring the power losses, the power can be calculated as

$$P_{in} = nV_{in}\frac{\int_0^{t_3} i_{Lr}(t)dt}{T_S/2} = P_o = \frac{V_o^2}{R_o} \qquad (12)$$

According to (1)~(9) and (12), the voltage conversion ratio can be derived as

$$G = \frac{1}{2}(1+\sqrt{1+\frac{\pi d_{\varphi S}^2}{2Q}}) \qquad (13)$$

where Qis the quality factor and defined as follow.

$$Q = \frac{Z_r}{R_o} \qquad (14)$$

b)*Buck Mode with Primary-Side Phase-Shift Control:*

When the converter works in the buck mode with G≤1 and primary-side phase-shift control, according to the operation principles and waveforms shown in Fig. 4.8 and Fig. 4.9, the power can be calculated as

$$P_{in} = nV_{in}\frac{\int_0^{t_2} i_{Lr}(t)dt}{T_S/2} = P_o = \frac{V_o^2}{R_o} \qquad (15)$$

According to (1)~(4), (8)~(11), and (14)~(15), the voltage conversion ratio can be derived as follows.

$$G = \frac{-B + \sqrt{B^2 - 4AC}}{2A} \tag{16}$$

Where,

$$A = 2\sqrt{2} / f_r \tag{17}$$

$$B = 2(\cos \pi d_{\varphi P} - 1)\left(\frac{1}{\sqrt{2} f_r} - \frac{1}{4\sqrt{2}\pi f_r Q}\right) \tag{18}$$

$$C = \frac{1}{2\sqrt{2}\pi f_r Q}(\cos \pi d_{\varphi P} - 1) \tag{19}$$

The normalized voltage conversion ratio curves versus the equivalent phase-shift duty-cycle with different quality factor, Q, are shown in Fig. 13.

It can be seen that buck mode with G<1 and boost mode with G≥1 are achieved by applying dual-phase-shift control to the RVMR-based RC. When $d_{\varphi P}$=1 and $d_{\varphi S}$=0, the normalized voltage ratio Gis unity and independent of Q, which is the same as a conventional series-resonant converter. In addition, higher voltage conversion ratio can be realized with a smaller Q.

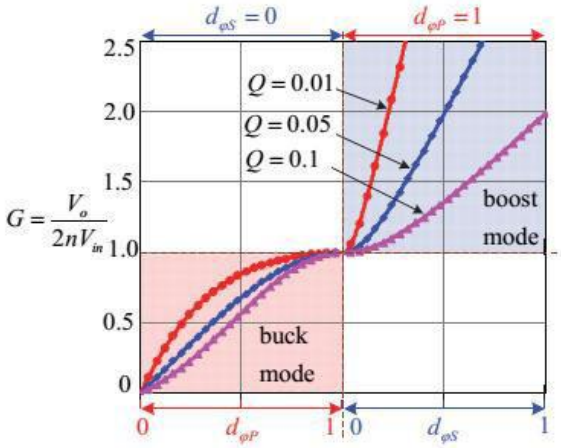

Fig 13: Normalized voltage gain versus phase-shift duty-cycle

B. Soft-Switching Performance:

According to the operation principles, ZVS of all of the active switches and ZCS of all of the diodes can be achieved with the unique structure of the proposed RVMR and RC topology and by using the constant-frequency phase-shift control. The soft-switching can be achieved regardless of input/output voltage or output power.

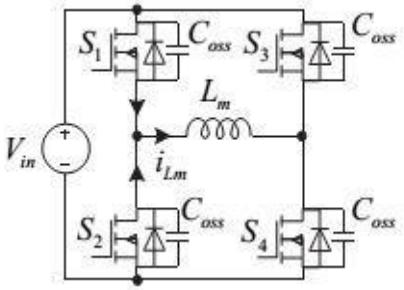

Fig 14: Equivalent circuits during the dead time

When analyzing the operation principles of the converter, the parasitic capacitance of the switches is ignored due to the limit of page-length. For the primary-side switches, the magnetizing inductance, L_m, of the transformer is used to discharge the parasitic drain-source capacitance of the primary side MOSFETs during the dead time to implement ZVS. Proper values of the magnetizing inductance and dead time should be selected to realize ZVS. If the parasitic capacitance is considered, the equivalent circuit of the primary-side circuit during the dead time is shown in Fig. 15. The peak current of magnetizing inductance L_m, when corresponding MOSFETs are turned OFF, is given by the following equation.

$$I_{Lm\_pk} = \frac{V_{in} d_{\varphi P} T_S}{4L_m} \tag{20}$$

When one switch capacitance is charged, the other switch capacitance in the same leg is discharged. So the equivalent capacitance in each leg is equal to two times of the capacitance of one of the MOSFETs, C_{oss}. Then, the ZVS condition of the primary-side MOSFET can be given by

$$I_{Lm\_pk} T_{DT} \geq 2C_{oss} V_{in} \tag{21}$$

According to (20) and (21), we have

$$L_m \leq \frac{d_{\varphi P} T_{DT} T_S}{8C_{oss}} \tag{22}$$

Where, $T_{DT}$is the dead-time. It can be seen that a tradeoff should be made between the magnetizing inductance and dead-time.

C. Design Guidelines:

A 40V-60V input 400V/400W-output prototype operating at 100 kHz switching frequency is adopted as an example to explore the main parameter design considerations. The main constraints for designing the parameters

of resonant tank, $L_r$and C_r, are resonant frequency and output power. The relationship between the voltage ripple on the resonant capacitance and the output power has been given in (9). The maximum voltage ripple should be lower than the DC voltage on the capacitor, which is equal to half of the output voltage. Therefore, the value of resonant capacitance should satisfy

$$C_r > \frac{P_o T_S}{2V_o^2} \quad (23)$$

Substituting V_O=400V, P_o=400W and T_S=10μs into (24), wehave C_r>12.5nF. According to (1) and (24), resonant inductor $L_r$should satisfy

$$L_r < \frac{V_o^2}{2\omega_r^2 P_o T_S} \quad (24)$$

Substituting the parameters into (24), then L_r<101μH. In practice, a larger C_r and smaller $L_r$will lower peak voltage on C_r, which would be better for reducing the peak voltage on the secondary-side active switches S_5, $S_6$and diodes D_1, D_4, because the voltage stresses on these devices are ($0.5V_o+\Delta V_{Cr}$).

But larger C_r will lead to large size and volume of the resonant capacitance. Taking the value of the actual capacitors into account, two 22nF capacitors are used as the resonant capacitors. According to (9), the peak voltage of S_5, $S_6$and D_1, $D_4$is about 414V and 400V-rated devices can be used.

Substituting the values of resonant capacitor and switching frequency into (1), the resonant inductor $L_r$should be 57.4μH. The input voltage is in a range of 40V-60V, and the normalinput voltage is 50V. The transformer turns ratio was selected to be n=4 according to the normal voltage to make the normalized voltage gain G=1 at V_{in}=50V. Then the highest efficiency can be achieved at this voltage, and the operation voltage ranges of the buck and boost modes are equal.

The magnetizing inductance $L_m$of the transformer is selected based on (22) to achieve ZVS for the primary-side switches. Minimum primary-side duty cycle $d_{\varphi P}$occurs when V_{in}=60V, according to the voltage gain curves shown in Fig. 13, $d_{\varphi P}$is about 0.6 at full-load when Vin=60V. According to the voltage and current stresses of primary-side switches, MOSFET with part number IPP052NE7N4, whose output capacitance C_{oss}≈1nF, is selected. Meanwhile, the dead-time TDTis set to 70ns, then the calculated result is L_m<52μH.

According to the voltage and current stresses on the secondary-side switches and diodes, 400V-rated diode with part number DPG40C400HB is used for $D_1$and D_4because the peak voltage on the two diodes is about 414V, while 600V-rated diode with part number DSEC40-06A is used for $D_2$and D_4because the voltage stress on the two diode is equal to the output voltage 400V. And the part number of secondary-side switches S_5 and $S_6$is IPx50R190CE. (4.23)

D. Implementation of Control:

This converter has two modes of operation that need to be regulated. This can be achieved using a two-carrier modulation technique. The control block diagram and principle of modulation are shown in Fig. 4.14 the phase-shift angles are determined only by the output of PI regulator, v_{ctrl}. The phase shift modulator consists of two carrier signals. $V_{m1}$is the amplitude of the buck mode carrier. When $v_{ctrl}$is lower than $V_{m1}$and compared with the buck mode carrier, the output of the modulator, $d_{\varphi P}$, is used to phase-shift modulate the primary side switches. (4.24)

The boost mode carrier is offset by V_{m1}. When $v_{ctrl}$is greater than $V_{m1}$and compared with this carrier, the output of the modulator, $d_{\varphi S}$, is used to phase-shift modulate the secondary side switches. In practice, the output regulation canbe realized easily by using an digital signal processor.

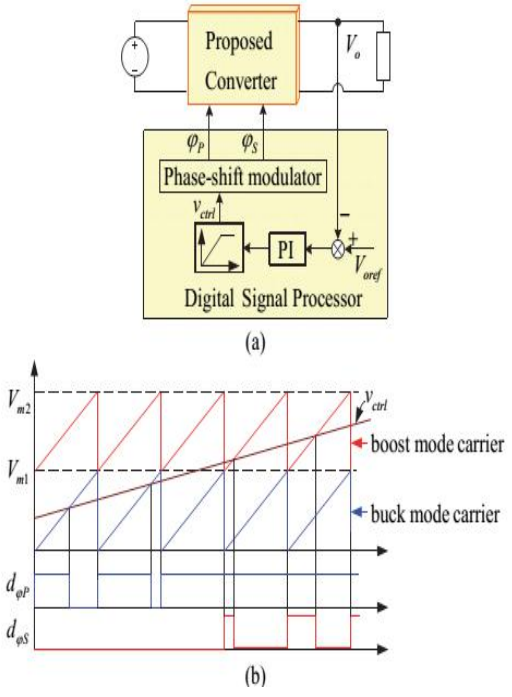

Fig 15: (a) control block diagram, (b) principle of modulation

E. Performance Comparison:

The conventional full-bridge LLC resonant converter shown in Fig. 16 is selected for performance comparison due to the similar characteristics. Since both the LLC converter and the existed converter can realize soft-switching for all of the switching devices, only the conduction losses are analyzed here.

The magnetizing inductance, Lm, of the LLC resonant converter has to be decreased to provide the desired voltage conversion ratio, so the circulating current introduced by the $L_m$is much larger than the proposed converter. The current stresses and conduction losses of the primary-side switches, transformer winding, resonant inductor and resonant capacitor are larger than the proposed converter, because the resonant tank is placed on the primary-side of the LLC resonant converter.

However, the conduction losses of the rectifier diodes of the LLC resonant converter are lower than the proposed converter, because additional two switches are employed in the proposed RVMR while only four diodes are used in the LLC resonant converter. Fortunately, the current of the secondary-side is much lower due to high output voltage, and the voltage stresses of the two upper diodes, $D_1$and D_4, and switches $S_5$and S_6 in the existed converter are lower than the rectifying diodes in the LLC resonant converter. Therefore, low voltage-rated diodes and switches with lower conduction losses and better switching performance can be used to reduce the power Losses.

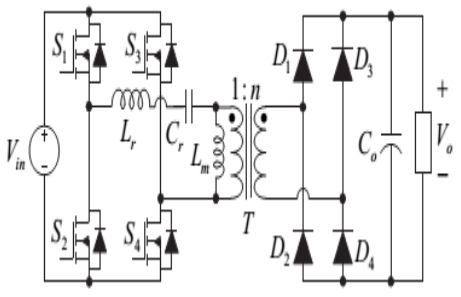

Fig 16. Full-bridge LLC resonant converter

In order to verify the performance of the proposed converter a model with a model has been developed with an isolated dc-dc conversion with a secondary control stage with a single source was built to verify the operation, the patterns and the wave forms of the proposed converters are been discussed.

V.CONCLUSION

In this paper, a high voltage gain dc-dc converter is introduced that can offer a voltage gain of 20,i.e.,to step-up a 20Vinput into 400V output.The proposed converter is mainly used forhigher harmonic voltages are filtered by the resonant network, a nearly sinusoidal current appears at the input of the resonant, which enables zero voltage switching (ZVS) or zero current switching (ZCS) of switching devices.An isolated Buck-Boost converter based on the isolated resonant converters , which can operate either in buck mode or boost mode could be more flexible than an isolated Buck or Boost converter in terms of conversion efficiency and voltage range, it is possible to achieve peak efficiency at the normal input voltage with a resonant Buck-Boost converter while not sacrificing the efficiency at the maximum or minimum input voltage which makes the utilization of the such resonant converters for a high step-up conversions.

VI.REFERENCE

[1] V. A. K. Prabhala, B. P. Baddipadiga, and M.

Ferdowsi, "DC distribution systems - An overview," *in Renewable Energy Research and Application (ICRERA), 2014 International Conference on,* 2014, pp.307-312.

[2] G. AlLee and W. Tschudi, "Edison Redux: 380 Vdc Brings Reliability and Efficiency to Sustainable Data Centers," *Power and Energy Magazine, IEEE*, vol. 10, pp. 50-59, 2012.

[3] V. Sithimolada and P. W. Sauer, "Facility-level DC vs. typical ac distribution for data centers: A comparative reliability study," in *TENCON 2010 - 2010 IEEE Region 10 Conference,* 2010, pp. 2102-2107.

[4] S. M. Lisy, B. J. Sonnenberg, and J. Dolan, "Case study of deployment of 400V DC power with 400V/-48VDC conversion," in *Telecommunications Energy Conference (INTELEC), 2014 IEEE 36th International*, 2014, pp. 1-6.

[5] A. Fukui, T. Takeda, K. Hirose, and M. Yamasaki, "HVDC power distribution systems for telecom sites and data centers," *in Power Electronics Conference (IPEC), 2010 International*, 2010, pp. 874-880.

[6] D. J. Becker and B. J. Sonnenberg, "DC microgrids in buildings anddata centers," in *Telecommunications Energy Conference (INTELEC), 2011 IEEE 33rd International*, 2011, pp. 1-7.

[7] E. Rodriguez-Diaz, M. Savaghebi, J. C. Vasquez, and J. M. Guerrero,"An overview of low voltage DC distribution systems for residential applications," in *Consumer Electronics - Berlin (ICCE-Berlin), 2015 IEEE 5th International Conference on*, 2015, pp. 318-322.

[8] W. Bin, L. Shouxiang, L. Yao, and K. M. Smedley, "A New Hybrid Boosting Converter for Renewable Energy Applications," *Power Electronics, IEEE Transactions on*, vol. 31, pp. 1203-1215, 2016.

[9] W. Gang, R. Xinbo, and Y. Zhihong, "Nonisolated High Step-Up DC-DC Converters Adopting Switched-Capacitor Cell," *Industrial Electronics, IEEE Transactions on,* vol. 62, pp. 383-393, 2015.

[10] T. Yu, W. Ting, and H. Yaohua, "A Switched-Capacitor-Based Active-Network Converter With High Voltage Gain," *Power Electronics, IEEE Transactions on*, vol. 29, pp. 2959-2968, 2014.

[11] J.C. Rosas-Caro, F. Mancilla-David, J. C. Mayo-Maldonado, J. M.Gonzalez-Lopez, H. L. Torres-Espinosa, and J. E. Valdez-Resendiz, "A Transformer-less High-Gain Boost Converter With Input Current Ripple Cancelation at a Selectable Duty Cycle," *Industrial Electronics, IEEE Transactions on*, vol. 60, pp. 4492-4499, 2013.

[12] W. Li and X. He, "High step-up soft switching interleaved boost converters with cross-winding-coupled inductors and reduced auxiliary switch number," *Power Electronics, IET,* vol. 2, pp. 125-133, 2009.

[13] L. Wuhua, X. Chi, Y. Hongbing, G. Yunjie, and H. Xiangning,"Analysis, design and implementation of isolated bidirectional converter with winding-cross-coupled inductors for high step-up and high step-down conversion system," *Power Electronics, IET*, vol. 7, pp. 67-77, 2014.

[14] A. Ajami, H. Ardi, and A. Farakhor, "A Novel High Step-up DC/DC Converter Based on Integrating Coupled Inductor and Switched-Capacitor Techniques for Renewable Energy Applications," *Power Electronics, IEEE Transactions on,* vol. 30, pp. 4255-4263, 2015.

[15] T. Kuo-Ching, H. Chi-Chih, and C. Chun-An, "A High Step-Up Converter With Voltage-Multiplier Modules for Sustainable Energy Applications," *Emerging and Selected Topics in Power Electronics, IEEE Journal of*, vol. 3, pp. 1100-1108, 2015.

[16] W. Hongfei, M. Tiantian, G. Hongjuan, and X. Yan, "Full-Range Soft-Switching-Isolated Buck-Boost

Converters
With Integrated Interleaved Boost Converter and Phase-
Shifted Control," *Power Electronics, IEEE Transactions on,* vol. 31, pp. 987-999, 2016.
[17] H. Xuefeng and G. Chunying, "A High Voltage Gain
DC-DC Converter Integrating Coupled-Inductor and
Diode-Capacitor Techniques," *Power Electronics, IEEE Transactions on*, vol. 29, pp. 789-800, 2014.
[18] L.Wuhua, L.Weichen, X. Xin, H.Yihua, and H.Xiangning,
"High Step-Up Interleaved Converter With Built-In
Transformer Voltage Multiplier Cells for Sustainable
Energy Applications," *Power Electronics, IEEE Transactions on,* vol. 29, pp. 2829-2836, 2014.
[19] V. A. K. Prabhala, P. Fajri, V. S. P. Gouribhatla, B. P.
Baddipadiga,and M. Ferdowsi, "A DC-DC Converter
With High Voltage Gain and Two Input Boost Stages,"
Power Electronics, IEEE Transactions on, vol. 31, pp.
4206-4215, 2016.
[20] B. R.Marshall, M. M. Morys, and G. D. Durgin,
"Parametric analysis and design guidelines of RF-to-DC
Dickson charge pumps for RFID energy harvesting," in
RFID (RFID), 2015 IEEE International Conference on,
2015, pp. 32-39.
[21] Baddipadiga, Bhanu Prashant, and Mehdi Ferdowsi. "A
High-Voltage-Gain DC–DC Converter Based on Modified Dickson Charge Pump Voltage Multiplier."
IEEE Transactions on Power Electronics 32.10 (2017):
7707-7715.